Electronic Research Archive

http://www.aimspress.com/journal/era

ERA, 32(3): 1533–1550
DOI: 10.3934/era.2024070
Received: 26 December 2023
Revised: 01 February 2024
Accepted: 03 February 2024
Published: 19 February 2024

Research article

Regulatory role of excitatory interneurons by combining electrical stimulation for absence seizures in the coupled thalamocortical model

Quanjun Wu, Zhu Zhang, Ranran Li, Yufan Liu and Yuan Chai*

School of Mathematics and Physics, Shanghai University of Electric Power, Shanghai 201306, China

* **Correspondence:** Email: chaiyuan@shiep.edu.cn.

Abstract: The role of excitatory interneurons (EINs) in the cortical has received increasing attention in the discussion of absence seizures. Numerous physiological experiments have confirmed the correlation between EIN and absence seizures. However, the dynamic mechanisms underlying this relationship are not well understood, and there are some challenges in selecting appropriate stimulation strategies for pyramidal clusters. In this study, we incorporated EIN into the previous Taylor model and developed an improved thalamocortical coupled model consisting of ten neuronal populations. Initially, we investigated the excitatory induction effect of EIN to pyramidal clusters and the external input of EIN. Then, four different targeted treatment approaches (deep brain stimulation (DBS), current balanced biphasic pulse (CBBP), 1:0 coordinated resetting stimulation (1:0 CRS), and 3:2 CRS) were applied to the pyramidal clusters. Moreover, we established two quantitative indices to evaluate the stimulation effects. The results showed that modifying the external input of EIN and the coupling strength projected onto the pyramidal clusters can effectively transition the system from an absence seizure state to other normal states. Additionally, inputs from the left compartment were found to reduce the generation of abnormal discharge regions in the right compartment. Furthermore, considering the treatment effects and current consumption, the 3:2 CRS stimulation strategy appeared to be the most suitable treatment approach for the pyramidal clusters. This work introduces a novel coupled model containing EIN, which contributes new theoretical foundations and insights for the future treatment of absence seizures.

Keywords: absence seizure; excitatory interneurons; coupled model; deep brain stimulation; coordinated reset stimulation

1. Introduction

Epilepsy is a prevalent paroxysmal disorder of the central nervous system, characterized by abnormal synchronous discharges of neurons in the brain. During disease episodes, patients with epilepsy experience insufficient blood and oxygen supply to the brain, resulting in cerebral tissue damage and

posing significant harm to the human body [1,2]. According to a report by the World Health Organization, more than 70 million people worldwide are currently affected by epilepsy, and this number continues to increase at a rate of 300,000–500,000 cases per year [3]. Absence seizures, a type of generalized seizure, originate simultaneously in both hemispheres of the brain and are characterized by their paroxysmal, recurrent, and brief nature [4, 5]. Absence seizures are mainly observed in the pediatric population and are typically accompanied by mild impairment of consciousness, resulting in transient memory gaps and motor disturbances [6, 7]. Furthermore, a characteristic rhythmic 2–4 Hz bilateral synchronous spike-and-wave discharges (SWDs) activity can be observed on the electroencephalogram (EEG) of individuals with typical absence seizures. Recurrent absence seizures inflict severe damage on the psychological and physical well-being of children. However, due to the complex nature of the nervous system and the interplay of various stochastic factors, the underlying mechanisms of absence seizures are not yet fully understood.

Computational models have emerged as crucial tools for investigating various neurological disorders in current research [8], and the thalamocortical model is a typical neural field model that describes the interactions between the cerebral cortex and the thalamus. The fundamental assumption of this model is that a closed loop circuit is formed between the cortex and the thalamus [9]. In this circuit, the cortex activates thalamic neurons by sending signals to the thalamus, while the thalamus regulates cortical activity by providing feedback signals to the cortex. This interaction is believed to play a crucial regulatory role in information processing, perception, and cognitive processes [10]. Taylor et al. extended and refined the thalamocortical circuit based on the neural field model proposed by Amari et al. and Wilson et al. [11–13]. The improved model encompasses four distinct neuronal populations, with the average membrane potential within the cortex serving as the chosen state variable. Notably, the study's findings suggest the potential significance of heterogeneous cortical connections in cortical focal regions, as they appear to play a pivotal role. Additionally, the revised model successfully replicated the distinct brainwave patterns observed during absence seizures and tonic-clonic seizures, thereby demonstrating its ability to capture the characteristic neurophysiological signatures of these epileptic events. In order to comprehend the interactions between the cortical-thalamic regions in the generation of SWD at a spatial scale, Goodfellow et al. and Taylor et al. developed spatially extended brain network models employing coupling and neural field models, respectively [14, 15]. These models were constructed to elucidate the interplay within the cortical-thalamic circuitry during the emergence of SWD. Liu et al. discussed the pathological mechanisms induced by alterations in the parameters associated with the thalamic reticular nucleus (TRN) [16]. The findings revealed that changes in the excitability of the TRN lead to distinct abnormal discharge patterns in the cortex, suggesting that the TRN is the pacemaker of absence seizures. Cao et al. discovered that by manipulating the inhibitory coupling strength between inhibitory interneurons (IN) and excitatory pyramidal neuron populations (PY) as a critical bifurcation parameter, the system transitions from the absence seizures to the tonic oscillations [17]. Yan et al. showed that increasing self-inhibition and external input to TRN could drive the system from an epileptic state to a normal state [18]. Wang et al. employed a mean-field model to investigate the combined regulatory effects of cortico-thalamic feedforward inhibition and thalamic relay nucleus (SRN) and TRN feedback inhibition on absence epilepsy [19]. The study demonstrated that the feedback microcircuitry plays a more significant role in inhibiting absence seizures. Therefore, SWD discharge state can be changed into other normal discharge state by adjusting the coupling strength and stimulation target.

An imbalance between excitatory and inhibitory functions is widely regarded as a significant con-

tributing factor to the occurrence of absence seizures. However, most of the previous biocomputational models primarily focused on inhibitory interneurons in the cortex. Recent studies have indicated that excitatory interneurons composed of astrocytes in the neocortex also play a crucial role in epileptic seizures [20]. The synchronized discharges of EIN have the potential to propagate epileptic activity throughout the brain, and EIN are believed to have a crucial role in both the initiation and propagation of SWD [21]. Tabatabaee et al. employed an extended neural mass model to investigate the coupling interactions between EINs and other neurons [22]. By altering the coupling strengths of GABAergic and glutamatergic receptors within EINs, the system undergoes a transition from a normal background firing state to an epileptic state. Yan et al. introduced EIN into thalamocortical model with self-inhibitory IN connections to investigate dominant role played by EIN in SWDs [23, 24]. Nevertheless, it is important to acknowledge that the regulatory mechanisms of EIN during absence seizures are not well understood within thalamocortical models, particularly in spatially extended models. Thus, further research is warranted to investigate these mechanisms comprehensively.

Compared to traditional pharmacological treatments and surgical interventions, neuromodulation intervenes, particularly DBS, have been proven to yield significant therapeutic effects with relatively low risk [25–27], which greatly promotes the application of DBS. The optimization of DBS strategies has recently received significant attention from researchers, particularly in terms of minimizing damage to brain tissue and reducing battery energy consumption while ensuring the effectiveness of the stimulation strategy. The goal is to strike a balance between achieving significant therapeutic effects and minimizing potential harm to the brain tissue and energy consumption from the stimulation. Yu et al. investigated the inhibitory effect of transcranial direct current stimulation on the propagation of epileptic activity in a large-scale epilepsy network model [28]. This constant low-intensity direct current has been shown to effectively reduce the seizure frequency in patients. Hou et al. applied the tri-phase delay stimulation on three neurons connected to the globus pallidus internal. By adjusting the stimulation parameters, this method exhibited a substitute effect similar to the regulation of the basal ganglia [29]. For refractory patients, CRS [30] and CBBP [31] were proposed as approaches to reconcile the conflicting goals of treatment efficacy and energy consumption. Both of these treatment approaches involve intermittent stimulation of target neurons on a temporal scale, aiming to reduce energy requirements and side effects. However, the selection of the optimal cortical stimulation strategy in coupled models remains unknown.

To overcome these limitations, we introduced EIN into the cortical region and designed a novel thalamocortical coupled model with two compartments. There are two main contributions in this study. On the one hand, by expanding the original thalamocortical model spatially, we were able to simulate brain activity more realistically. We discovered that by adjusting the excitatory coupling strength from EIN to PY and the external input of EIN, it was possible to internally suppress the generation of pathological states without the need for external stimulation. On the other hand, we applied four different electrical stimulation strategies in the cortical region to explore the optimal external stimulation scheme to counteract absence seizures. We hope this study could provide new perspectives for the clinical treatment of absence seizures in epilepsy.

The current article is organized as follows. In the second section, we advance the improvement of the thalamocortical model by introducing EIN and present the employed electrical stimulation paradigm. In the third section, we analyze the predominant role of EIN in inducing SWD and examine the diverse effects of different stimulation strategies on suppressing SWD generation and energy consumption. Finally, we apply DBS separately to the left and right compartment to elucidate the critical role of

stimulation in the coupled model. In the fourth section, we summarize the obtained results and engage in a discussion regarding the prospective avenues for future research.

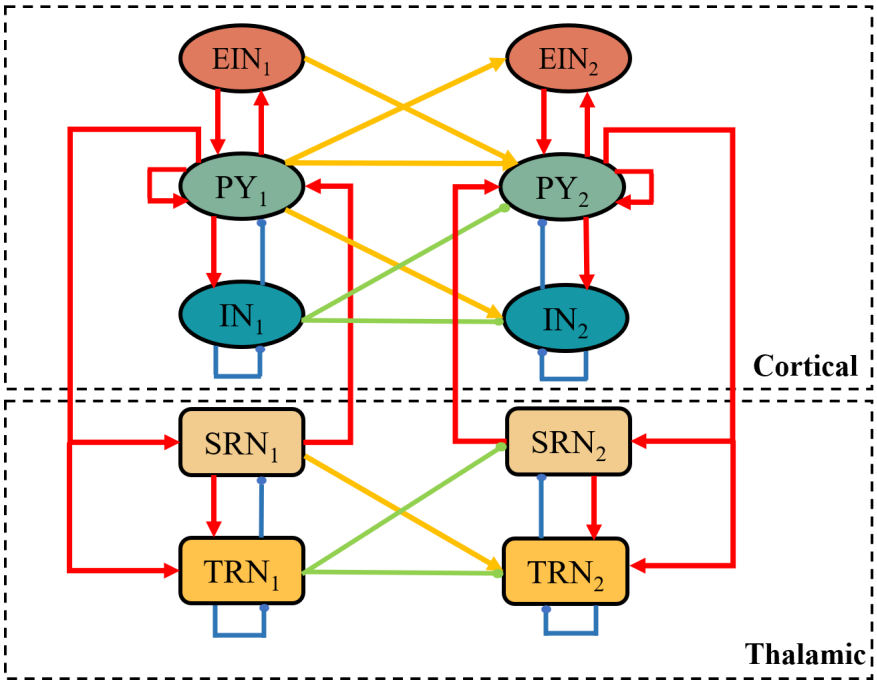

Figure 1. Schematic diagram of the coupled thalamocortical model. The model consists of ten clusters of five types of neurons, which is composed of EIN, PY, and IN in the cortex, as well as SRN and TRN in the thalamic. The excitatory synapses mediated by glutamate are represented by lines with arrows, while inhibitory synapses mediated by gamma-aminobutyric acid (GABA) are depicted by closed circles.

2. Models and stimulus description

2.1. Description of model

The thalamocortical circuit model consists of two interacting modules: the cortical module, which primarily includes PY and IN, and the thalamic module, composed of TRN and SRN. In this study, we have built upon the neural field model proposed by [15] and made modifications to investigate the impact of spiny stellate cells on seizure activity. Specifically, we introduced excitatory EIN in the cortical module, which are connected to PY by glutamate receptors. Also, the model was expanded to a 2-compartment coupled model to simulate more realistic cortical discharge dynamics and transitions among different oscillation states. Additionally, we incorporated self-inhibition in the IN as well. The schematic of coupled model with EIN is formulated as shown in Figure 1. The proposed model maintains consistency with the physiological connectivity framework of the thalamocortical circuit [9]. Excitatory synapses mediated by glutamate are represented by lines with arrows, while inhibitory synapses mediated by gamma-aminobutyric acid (GABA) are depicted by closed circles.

Generally, the coupled model equations, which govern the behavior of the system, can be described

as follows:

$$\frac{dPY_1}{dt} = \tau_1(h_{PY} - PY_1 + C_{PY-PY}f[PY_1] + C_{EIN-PY}f[EIN_1] - C_{IN-PY}f[IN_1] + C_{SRN-PY}f[SRN_1]) + k_1(t)u(t), \tag{1}$$

$$\frac{dIN_1}{dt} = \tau_2(h_{IN} - IN_1 + C_{PY-IN}f[PY_1] - C_{IN-IN}f[IN_1]), \tag{2}$$

$$\frac{dEIN_1}{dt} = \tau_3(h_{EIN} - EIN_1 + C_{PY-EIN}f[PY_1]), \tag{3}$$

$$\frac{dSRN_1}{dt} = \tau_4(h_{SRN} - SRN_1 + C_{PY-SRN}f[PY_1] - C_{TRN-SRN}g[TRN_1]), \tag{4}$$

$$\frac{dTRN_1}{dt} = \tau_5(h_{TRN} - TRN_1 + C_{PY-TRN}f[PY_1] + C_{SRN-TRN}g[SRN_1] - C_{TRN-TRN}g[TRN_1]), \tag{5}$$

$$\begin{aligned}\frac{dPY_2}{dt} =& \tau_1(h_{PY} - PY_2 + C_{PY-PY}f[PY_2] + C_{EIN-PY}f[EIN_2] - C_{IN-PY}f[IN_2] + C_{SRN-PY}f[SRN_2]) \\ &+ \frac{C_{PY-PY}}{3}f[PY_1] + \frac{C_{EIN-PY}}{3}f[EIN_1] + \frac{C_{IN-PY}}{3}f[IN_1] + k_2(t)u(t),\end{aligned} \tag{6}$$

$$\frac{dIN_2}{dt} = \tau_2(h_{IN} - IN_2 + C_{PY-IN}f[PY_2] - C_{IN-IN}f[IN_2]) + \frac{C_{PY-IN}}{3}f[PY_1] - \frac{C_{IN-IN}}{3}f[IN_1], \tag{7}$$

$$\frac{dEIN_2}{dt} = \tau_3(h_{EIN} - EIN_2 + C_{PY-EIN}f[PY_2]) + \frac{C_{PY-EIN}}{3}f[PY_1], \tag{8}$$

$$\frac{dSRN_2}{dt} = \tau_4(h_{SRN} - SRN_2 + C_{PY-SRN}f[PY_2] - C_{TRN-SRN}g[TRN_2]) - \frac{C_{TRN-SRN}}{3}g[TRN_1], \tag{9}$$

$$\begin{aligned}\frac{dTRN_2}{dt} =& \tau_5(h_{TRN} - TRN_2 + C_{PY-TRN}f[PY_2] + C_{SRN-TRN}g[SRN_2] \\ &- C_{TRN-TRN}g[TRN_2]) + \frac{C_{SRN-TRN}}{3}g[SRN_1] - \frac{C_{TRN-TRN}}{3}g[TRN_1],\end{aligned} \tag{10}$$

where $PY_{1,2}$, $IN_{1,2}$, $EIN_{1,2}$, $SRN_{1,2}$, and $TRN_{1,2}$ represent five types of neuron populations in the coupled model as mentioned above; τ_1, τ_2, τ_3, τ_4, and τ_5 are time scale parameters; h_{PY}, h_{IN}, h_{EIN}, h_{SRN}, and h_{TRN} denote the external inputs; $C_{PY-PY}, C_{EIN-PY}, ..., C_{TRN-TRN}$ represent the coupling strengths among different populations of neurons; and $f[\cdot]$ and $g[\cdot]$ are denoted to activation functions with the following form:

$$f[x] = \frac{1}{1 + \omega^{-x}}, \tag{11}$$

$$g[y] = \alpha y + \beta, \tag{12}$$

where $x = PY_{1,2}, IN_{1,2}, EIN_{1,2}, y = SRN_{1,2}, TRN_{1,2}$; ω and α determine the steepness of two activation functions; β is set to 0.5 as a constant; $k_{1,2}$ represent the control variables; and $u(t)$ denotes the various stimulation input.

The spatially expanded two-compartments coupled model is one of the fundamental thalamocortical network models. It has a relatively simple structure but carries physiological significance. In this model, cells in each layer are arranged in a one-dimensional manner. This one-dimensional network model, consisting of five cell types, greatly simplifies the multi-layered structure of the thalamocortical system without requiring additional complexity and has been widely applied [32, 33]. Furthermore, the PY in

the cortex possess axons of sufficient length, enabling them to exert significant propagative effects on distant neuronal populations, whereas other neuronal clusters with shorter axons can only influence neighboring regions [27]. Consequently, based on the distance between two compartments, there are three different types of inter-compartment connections: short-range connection, long-range connection, and distant excitatory connection. Since we are specifically considering the transmission projections within the same subsystem and these two compartments can only respectively affect the adjacent regions of the cerebral cortex and thalamus, short-range connection $C_i/3$ is employed in our model.

The parameters in the model remain consistent with previous studies [11, 23, 27] and have been fine-tuned within a reasonable range, and most of them are derived from clinical experiments, shown in Table 1.

Table 1. Values of parameters in this work.

Parameters	Interpretation	Value	Parameters	Interpretation	Value
C_{PY-PY}	PY→PY	1.8	h_{PY}	Input PY	-0.5
C_{EIN-PY}	EIN→PY	Scanned	h_{IN}	Input IN	-3.3
C_{IN-PY}	IN→PY	1.5	h_{EIN}	Input EIN	Scanned
C_{SRN-PY}	SRN→PY	1	h_{SRN}	Input SRN	-2.2
C_{PY-IN}	PY→IN	4	h_{TRN}	Input TRN	-5
C_{IN-IN}	IN→IN	0.12	τ_1	PY timescale	26
C_{PY-EIN}	PY→EIN	0.1	τ_2	IN timescale	32.5
C_{PY-SRN}	PY→SRN	4.2	τ_3	EIN timescale	26
$C_{TRN-SRN}$	TRN→SRN	0.4	τ_4	SRN timescale	2.6
C_{PY-TRN}	PY→TRN	2	τ_5	TRN timescale	2.6
$C_{SRN-TRN}$	SRN→TRN	17	ω	constant	250,000
$C_{TRN-TRN}$	TRN→TRN	0.1	α	constant	2.8

2.2. *Different stimulus strategies*

Electrical stimulation has emerged as an effective method in neural surgery and is widely employed in medicine, particularly for the treatment of epilepsy and movement disorders [34]. In our study, we utilize four distinct stimulus patterns to regulate SWD and induce transitions between different states, as shown in Figure 2.

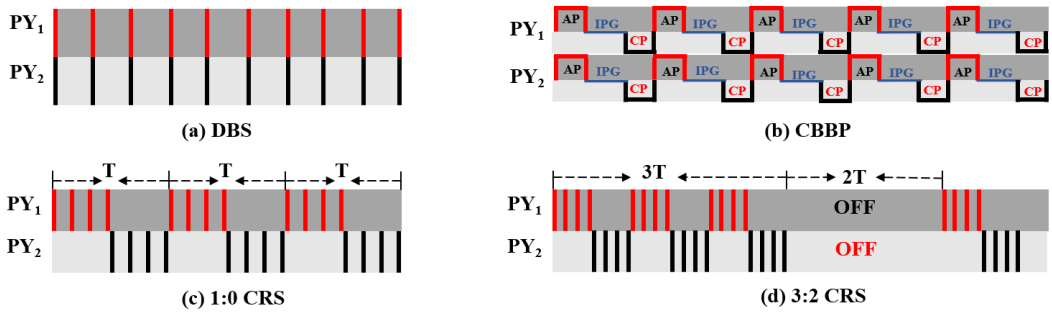

Figure 2. Overview of four types of stimulus strategies.

The first one is classical DBS, which has been successfully applied in the treatment of neurological disorders such as epilepsy and Parkinson's disease [35–37]. DBS involves the continuous and simultaneous delivery of electrical pulses to the PY_i to achieve therapeutic effects. The operational principle can be described as follows [38]:

$$u_{DBS}(t) = \alpha \times H(\sin(2\pi t f)) \times (1 - H(\sin(2\pi(t+\delta)f))), \tag{13}$$

where α is the amplitude of the oscillation, f represents the frequency and δ denotes pulse width, indicating the duration of the electrical pulse, and H represents the Heaviside bi-value function, that is, $H(x) = 1$,if $x > 0$, $H(x) = 0$,if $x \leq 0$.

The CBBP therapeutic plan has anodic pulse (AP), cathodic pulse (CP), and a rectangular waveform with appropriate inter-phase gap (IPG, note that $IPG^{max} = 1/f - 2\delta$), which can be described as follows [31]:

$$\begin{aligned} u_{\mathrm{CBBP}}(t) =& \alpha \times H(\sin(2\pi t f)) \times (1 - H(\sin(2\pi(t+\delta)f))) \\ & - \alpha \times H(\sin(2\pi(t - IPG - \delta)f)) \times (1 - H(\sin(2\pi(t - IPG)f))). \end{aligned} \tag{14}$$

In the CRS therapeutic plan, the m:n ON-OFF CRS signal added to $PY_{1,2}$ can be mathematically represented as follows [39]:

$$u_{CRS}(t) = k_1(t)u(t) + k_2(t)u(t), \tag{15}$$

where $k_1(t)$ and $k_2(t)$ represent the stimulation microelectrodes, which are index functions, and $k_{1,2}(t) = 0$ and 1 represent the opening and closing of the electrode, indicating the start and end of the stimulation respectively.

2.3. Numerical simulation methods and data analysis

In this study, all simulation were compiled and accomplished in MATLAB 2021a (Math works, USA) coding environment. In addition, we solved all the differential equations by standard fourth-order Runge-Kutta iterative method. The time window is set to 30 s and the selection of integration step is 0.25 ms, which was sufficiently small to ensure the accuracy of data acquisition. To ensure the system was in a stable state, data analysis commenced from the 27th second. In order to plot the extrema graph, the maximum and minimum values of the cortical discharge time series were calculated during the stable state. Fast Fourier transform (FFT) was utilized to extract the dominant frequency, represented by the peak frequency in the power spectral density, as the principal frequency.

3. Numerical results

3.1. Spontaneous epilepsy activities and transitions modulated by excitatory interneurons

Bidirectional connections between EIN and PY mediated by glutamatergic excitatory synapses are not static in terms of synaptic coupling strength. Changes in the release of neurotransmitters from both excitatory and inhibitory neurons in the brain can lead to short-term or long-term modifications in coupling strength [40, 41]. Certain antiepileptic drugs can modulate the activity of glutamate receptors, resulting in alterations in glutamatergic neurotransmission [42]. Additionally, in physiological experiments, functional alterations in glutamate receptors in the cerebral cortex of rats have been

observed to induce epileptic seizures [43]. However, the dynamics and mechanisms underlying the transition to seizure states induced by EIN are currently not well understood. In this section, we investigate the predominant role of EIN in generating absence seizures by changing external input and the coupling strength to PY. We first conducted the extrema analysis of the excitatory coupling strength from EIN to PY C_{EIN-PY} and the external inputs h_{EIN}. As we know, EEG data is collected by recording the collective electrical activity of neuronal populations within a specific region of the brain. In our model, the cortical module includes PY, IN, and EIN populations. Therefore, by calculating the average field potential of the neuronal populations in the cortex, our computational model can better simulate the cortical discharge activity. In this section, we primarily focus on the analysis of the left compartment in the coupled model, $(PY_1 + IN_1 + EIN_1)/3$.

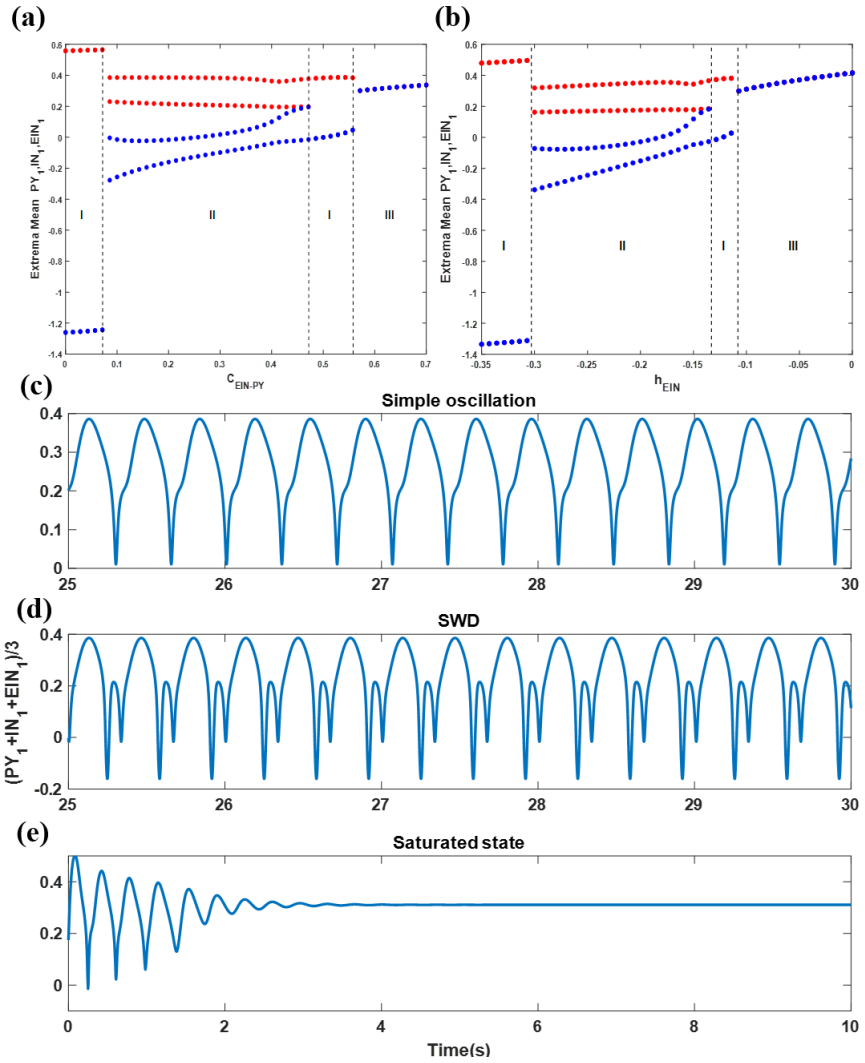

Figure 3. The extreme diagram showing the extrema mean of PY, IN, and EIN. When the fixed value h_{EIN} = -0.1, the system in (a) experiences three different states in the left compartment with gradual increase of C_{EIN-PY}, namely simple oscillation, SWD, and saturated state. When C_{EIN-PY} = 0.6, three states appear in (b), which is similar to (a). The time series of $(PY_1 + IN_1 + EIN_1)/3$ are shown in (c–e), respectively.

Figure 3(a),(b) display the results of extrema analysis, revealing three distinct dynamical states. The corresponding time series can be observed in Figure 3(c)–(e). When the coupling strength C_{EIN-PY} is small, the activation level of PY is largely independent of the control exerted by EIN and the system is in a simple oscillation state. The corresponding frequency is similar to absence seizures, but the amplitude is much larger. When C_{EIN-PY} increases, EIN gradually induces the activation of PY and the excitability level of the cortex begins to increase. As shown in Figure 3(d), two peaks can be observed, indicating the presence of typical SWD, characterized by the periodic occurrence of two maxima and minima. This pattern signifies the onset of absence seizure activity. Finally, as coupling strength C_{EIN-PY} constantly increases, the system exhibits a transient period of brief oscillatory activity again, but this time with significantly smaller amplitudes. Subsequently, the system enters a saturated firing state.

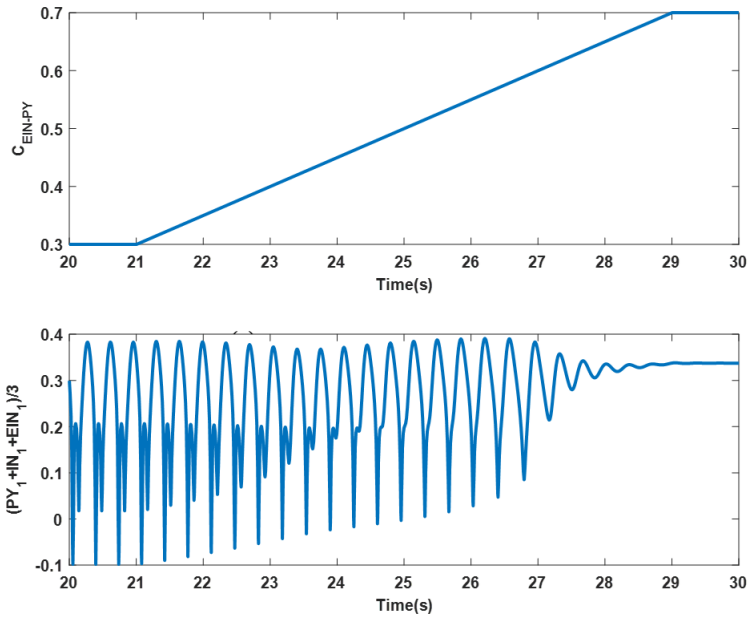

Figure 4. The changes of cortical firing rate with linearly increasing C_{EIN-PY}.

In order to observe the changes in cortical discharge more clearly during the variation of the coupling strength C_{EIN-PY}, we linearly increase C_{EIN-PY} over the time range of 21–29 s to explore the dynamic changes during absence seizures. Figure 4(b) shows that as the coupling strength C_{EIN-PY} increases, the cortical discharge pattern transitions from SWD (II) to simple oscillations (I). This indicates that normal brain activity relies on maintaining the stability of the excitatory level in the EIN-PY pathway and any disruption in the stability of the EIN-PY coupling strength may lead to the onset of absence seizures.

Because of the essential effect of EIN, we then fix the coupling strength from EIN to PY and set the external input to EIN h_{EIN} as the crucial parameter to explore the transitions between different states. As shown in Figure 3(b), we obtain four similar dynamic states to those in Figure 3(a), with the SWD region exhibiting two pairs of maxima and minima.

To validate whether the obtained simulation results can be generalized within a certain parameter range, we further conduct a two-dimensional state analysis in the (C_{EIN-PY}, h_{EIN}) plane. As shown in Figure 5(a), the entire panel is divided into four regions corresponding to the three states analyzed above. As expected, we find that the SWD state can only be produced within specific ranges of C_{EIN-PY} and h_{EIN}.

By appropriately adjusting C_{EIN-PY} and h_{EIN}, the system can transition from the epileptic state to the normal state. This result aligns with our previous conclusions, indicating the generality of the analysis.

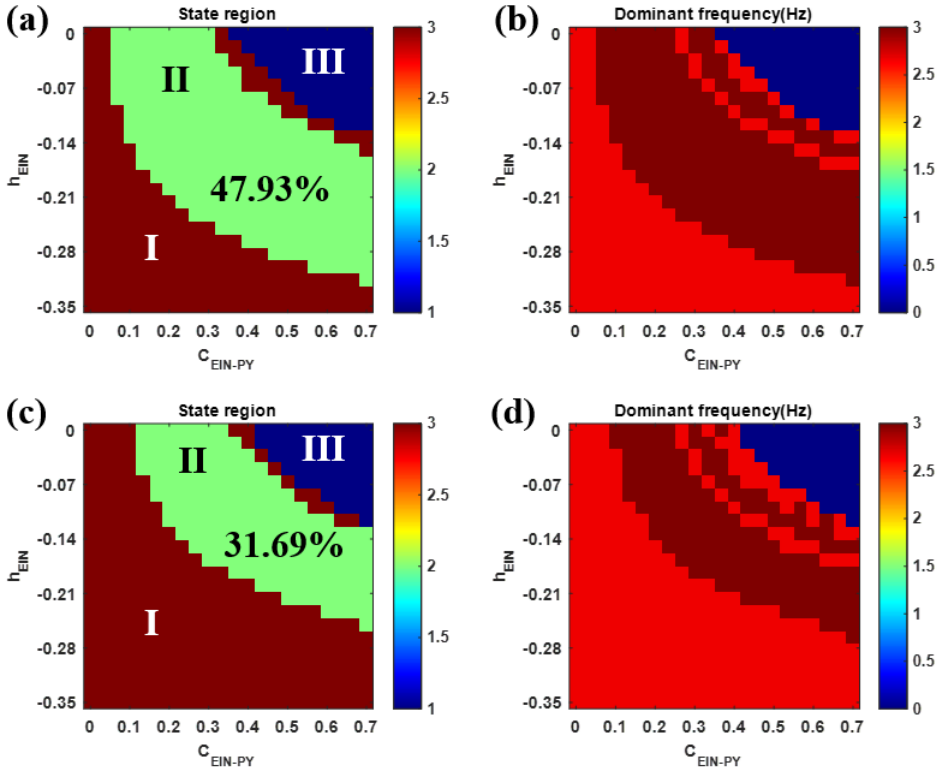

Figure 5. Dynamic analysis in the panel (C_{EIN-PY}, h_{EIN}) and their corresponding dominant frequency. (a) and (b) represent the left compartment and (c) and (d) represent the right. The region I represents the simple oscillation state, region II represents the state of SWD denoting absence seizures, and III represents the saturated state, corresponding the dark blue region in (b) and (d).

The model constructed in this study can reproduce typical absence seizure scenarios using previously validated pathological mechanisms. Figure 5(c),(d) illustrate the spatial distribution of the right compartment states and the corresponding dominant frequency plot in the coupled model. It can be observed that, in the absence of external stimulation, the area of SWDs generated by the right compartment is significantly smaller than that of the left compartment. The occurrence of absence seizures requires a relatively larger h_{EIN}, indicating that the connections from the left compartment can suppress the generation of SWDs in the right compartment. This finding provides evidence for the positive regulatory role of internal connections in the manifestation of absence seizures in the coupled model. Since we did not alter the normal parameter values in other regions during the above discussion, our results also suggest that abnormal changes in excitatory interneurons may contribute to the absence seizures.

3.2. Therapeutic effects of the four different stimulation strategies

Currently, the primary modality for treating epilepsy is medication. However, it is worth noting that approximately one-third of epilepsy patients fail to achieve seizure control through medication

alone, and the majority of individuals require ongoing medication or alternative treatments. Also, surgical resection of epileptogenic foci poses certain risks [44]. Therefore, doctors have gradually started adopting neurostimulation therapy as a replacement for the aforementioned approaches. As the core neurons in the cortex, the appropriate stimulation of PY populations to achieve optimal therapeutic effects remains unknown. In this section, we will apply four different stimulation protocols to PY populations to evaluate the most suitable therapeutic approach.

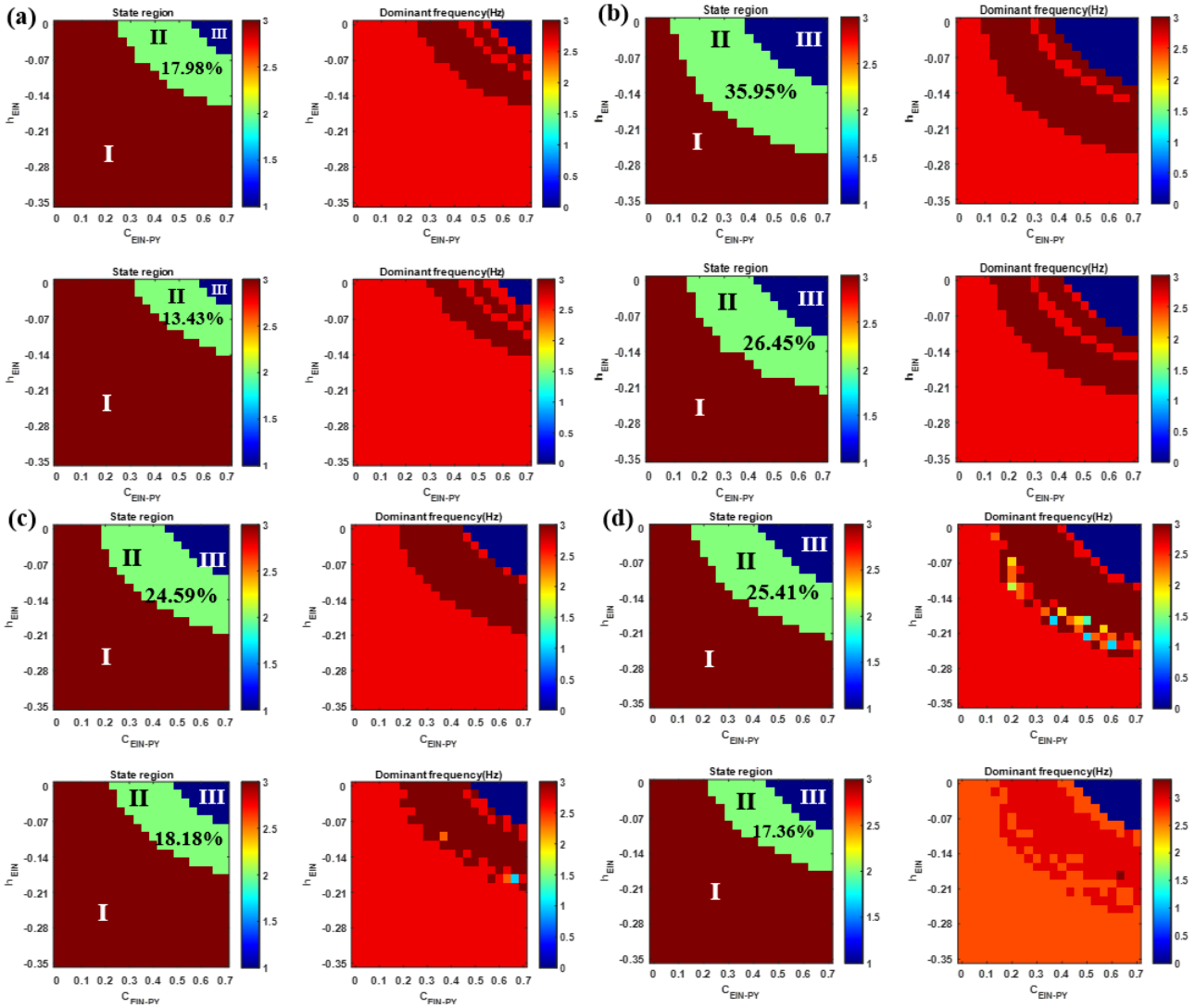

Figure 6. Comparison diagrams among four different stimulation strategies in left and right compartment respectively. Stimulation parameters are $\alpha = 8mA$, the positive input pulse $\delta = 4ms$, and frequency $f = 130Hz$. Two-dimensional dynamical evolution and corresponding are displayed through adding (a) DBS, (b) CBBP, (c) 1:0 CRS, and (d) 3:2 CRS respectively.

The implementation details of the DBS, CBBP, 1:0 CRS, and 3:2 CRS strategies are depicted in Figure 2. In order to facilitate the observation of SWD reduction through stimulations, we discretize the parametric plane into a grid of evenly spaced points. This allows us to quantify the grid points that correspond to the occurrence of SWD in the model. To quantitatively evaluate the effectiveness of the

stimulus in mitigating SWD, we employ the SWD control percentage as a metric:

$$\eta = (1 - S/P) \times 100\%, \tag{16}$$

where S and P represent the number of SWDs in the absence after applying stimulation to the neurons and in the original state respectively. Furthermore, to comprehensively evaluate different stimulation patterns, we also considered the current consumption as follows:

$$Q(t) = \int_0^{\mathrm{T}} \sum_{i=1,2} |u_i(t)| dt, \tag{17}$$

with the unit of $V \cdot s$. In our study, T=30 s is the stimulation duration.

The two-dimensional panel (C_{EIN-PY}, h_{EIN}) illustrates the changes in SWD regions and dominant frequencies after incorporating the four stimulation strategies. In particular, in Figure 6, the dark red and dark blue regions represent the states of simple oscillation and saturation state, respectively. The green region means the SWD oscillation during absence seizure, as shown in the dominant frequency plot, the pathological oscillations are within the range of 2–4 Hz. The corresponding frequency analysis is also displayed in Figure 6.

Compared to the original 47.93% SWD region in the left compartment and 31.61% in the right compartment shown in Figure 4, it can be observed that all four stimulation strategies result in varying degrees of contraction in the green SWD region. After adding DBS, the contraction of the SWD region is the most significant. In this case, the size of the SWD region in the right compartment is only 13.43%. The therapeutic effects of applying 1:0 CRS and 3:2 CRS are almost similar, with the proportion of SWD in the right compartment being 24.59 and 25.41%, respectively. The 1:0 CRS strategy is slightly better than 3:2 CRS. Finally, the CBBP stimulation strategy results in SWD regions accounting for 35.95% in the left compartment and 26.45% in the right compartment.

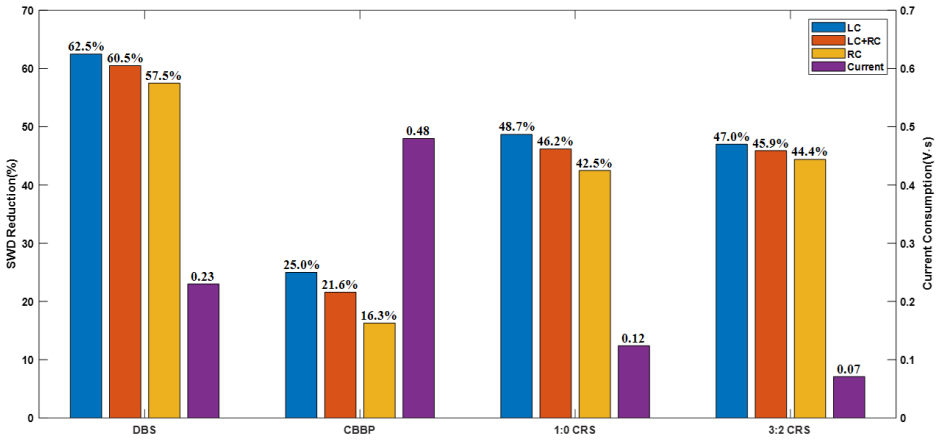

Figure 7. SWD reduction and current consumption after adding stimulations.

In order to gain a clearer understanding and compare the therapeutic effects of four stimulation strategies, we measured the percentage reduction of SWDs and the average current consumption as quantitative indicators. As shown in Figure 7, the blue and yellow bars represent the percentage reduction of absence seizure regions after stimulation in the left compartment and right compartment,

respectively, while the orange bar represents the average reduction ratio of both. The purple bar graph represents the average current consumption. From the graph, it can be observed that DBS yields the most optimal inhibitory effect on epileptic seizure states, with an average reduction rate of 60.5%. The 1:0 CRS and 3:2 CRS stimulation strategies exhibit comparable inhibitory effects on epilepsy, reducing seizures by 46.2 and 45.9%, respectively. In contrast, there was only 21.6% reduction with the CBBP stimulation strategy. Despite requiring the highest consumption of current, CBBP performed the least effectively among the four approaches. Despite DBS achieving the best inhibitory effect, it consumes a relatively larger amount of stimulation current. Clinical studies have confirmed that excessive current usage and sustained stimulation targeting a single specific target can have adverse effects on the human brain, leading to brain tissue damage and a range of neurological complications [45]. From the graph, it can be observed that although the 3:2 CRS strategy is slightly inferior to the 1:0 CRS strategy, it ranks highest in terms of current consumption among the four stimulation strategies while maintaining the highest inhibitory efficiency. Therefore, considering safety and comprehensiveness, the 3:2 CRS strategy is the most suitable for stimulating PY populations to achieve the purpose of inhibiting absence seizures.

3.3. Propagation effects of stimulation in coupled model

In the previous section, we applied stimulation to both the left and right compartments. DBS demonstrated the most effective therapeutic outcome by significantly reducing the area of seizures. The 3:2 CRS showed a balance between therapeutic effects and current consumption. However, it remains unknown whether the reduction in the right compartment area is due to the propagation of stimulation from the left compartment to the right, or if it is solely attributable to the corresponding stimulation applied to the right compartment. Given that DBS yielded the most pronounced inhibitory effect, this section will focus on exploring the specific reasons for the reduction in the right compartment area under the influence of DBS.

Figure 8 illustrates the changes in the right compartment seizure area when DBS is applied exclusively to the left compartment or the right. When DBS is applied exclusively to the left compartment, the proportion of right compartment SWDs is 28.47%. Compared to the initial state of the right compartment in Figure 5(c), its area decreases by 3.22%. On the other hand, when stimulation is applied exclusively to the right compartment, the SWD area is 16.98%. Compared to the simultaneous stimulation of both compartments, its area increases by 3.65%. These results suggest that in the unidirectional flow-coupling model, the reduction in the right compartment seizure area after DBS is predominantly driven by DBS itself. It indicates that the therapeutic effects generated by electrical stimulation are difficult to flow from the left compartment to the right. The above results highlight the crucial role of DBS in reducing the seizure area in the right compartment.

4. Conclusions

This study aimed at exploring the crucial role of excitatory interneurons in absence seizure activity. Building upon the Taylor model, we developed a spatially extended thalamocortical coupled model and four different electrical stimulation methods were applied to the model such as DBS, CBBP, 1:0 CRS, and 3:2 CRS. The major findings of this work are as follows: by adjusting the coupling strength between external inputs and the excitatory pathway of EIN to PY, we are able to induce transition from the normal physiological state of the cortical network to SWD, indicating that EIN are highly likely to

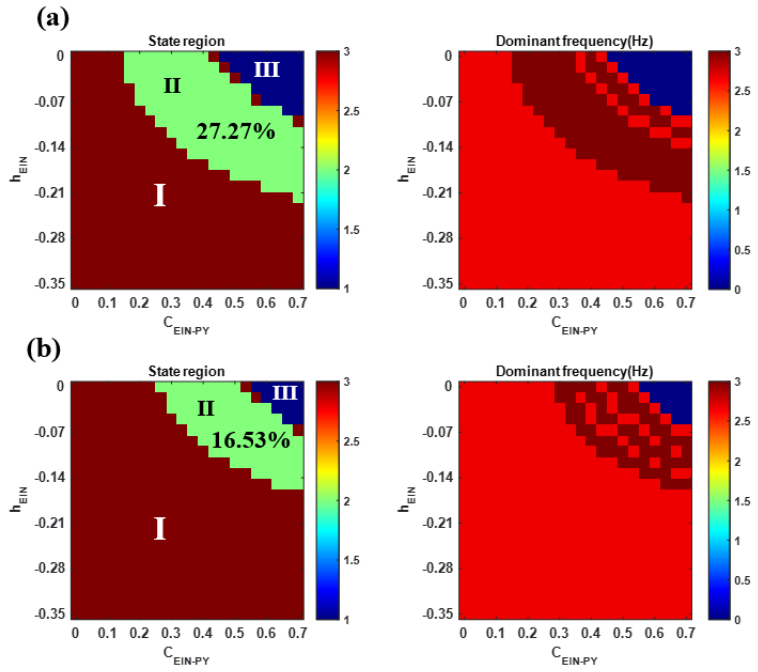

Figure 8. Propagation effects of DBS in the coupled model. (a) represents the case where DBS is applied only to the left compartment, resulting in a SWD area ratio of 27.27% in the right compartment, slightly smaller than the non-stimulated state. (b) represents the case where DBS is applied only to the right compartment, resulting in a SWD area of 16.53%, slightly smaller than when stimulation is applied simultaneously.

be the epileptic focus responsible for absence seizures. Furthermore, under the influence of the coupling model, projections from the left compartment can be found to significantly reduce the SWD region in the right compartment, which provides a novel approach for the internal modulation of absence epilepsy treatment. Subsequently, we evaluate the therapeutic effects of four stimulation methods applied on PY and conducted a quantitative comparative analysis to explore the optimal protocol. The 3:2 CRS achieves the best balance between therapeutic effects and current consumption in the coupled model, thus suggesting it as the most suitable stimulation method for this model. Ultimately, we observed that the therapeutic effects induced by stimulation face challenges in propagation through the connections between coupled models. Therefore, it becomes imperative to simultaneously apply stimulation to both the left and right compartments. We hope that our findings can provide insights for the treatment of absence epilepsy.

It is important to acknowledge certain limitations in this study. First, while our simulations demonstrated the involvement of EIN in the onset and offset of absence seizures, we provided only computational evidence. Further validation through physiological experiments would enhance the persuasiveness of our findings. Second, this study solely focused on PY as the target for stimulation, although multiple studies have shown the critical role of the TRN in regulating absence seizure activity. While PY are more amenable to electrode implantation compared to TRN, continuous stimulation of a single target may not be favorable. Future investigations could consider alternating stimulation between PY and TRN to potentially achieve better therapeutic outcomes.

Use of AI tools declaration

The authors declare they have not used Artificial Intelligence (AI) tools in the creation of this article.

Acknowledgments

This work was supported by the National Natural Science Foundation of China (Grant No. 11502139). The authors would like to thank the anonymous referees for their valuable comments.

Conflict of interest

The authors declare there is no conflicts of interest.

References

1. Y. Yu, F. Han, Q. Wang, A hippocampal-entorhinal cortex neuronal network for dynamical mechanisms of epileptic seizure, *IEEE Trans. Neural Syst. Rehabil. Eng.*, **31** (2023), 1986–1996. https://doi.org/10.1109/TNSRE.2023.3265581
2. E. Akyuz, A. K. Polat, E. Eroglu, I. Kullu, E. Angelopoulou, Y. N. Paudel, Revisiting the role of neurotransmitters in epilepsy: An updated review, *Life Sci.*, **265** (2021), 118826. https://doi.org/10.1016/j.seizure.2013.01.008
3. R. D. Thijs, R. Surges, T. J. O'Brien, J. W. Sander, Epilepsy in adults, *Lancet*, **393** (2019), 689–701. https://doi.org/10.1016/S0140-6736(18)32596-0
4. S. Gregorčič, J. Hrovat, N. Bizjak, P. Z. Rener, T. Hostnik, B. Stres, et al., Difficult to treat absence seizures in children: A single-center retrospective study, *Front. Neurol.*, **13** (2022), 958369. https://doi.org/10.3389/fneur.2022.958369
5. Z. W. Wong, T. Engel, More than a drug target: Purinergic signalling as a source for diagnostic tools in epilepsy, *Neuropharmacology*, **222** (2023), 109303. https://doi.org/10.1016/j.neuropharm.2022.109303
6. R. S. Fisher, C. Acevedo, A. Arzimanoglou, A. Bogacz, J. H. Cross, C. E. Elger, et al., ILAE official report: a practical clinical definition of epilepsy, *Epilepsia*, **55** (2014), 475–482. https://doi.org/10.1111/epi.12550
7. J. Xue, P. Gong, H. Yang, X. Liu, Y. Jiang, Y. Zhang, et al., Genetic (idiopathic) epilepsy with photosensitive seizures includes features of both focal and generalized seizures, *Sci. Rep.*, **8** (2018), 6254. https://doi.org/10.1038/s41598-018-24644-0
8. Z. Liu, F. Han, Q. Wang, A review of computational models for gamma oscillation dynamics: from spiking neurons to neural masses, *Nonlinear Dyn.*, **108** (2022), 1849–1866. https://doi.org/10.1007/s11071-022-07298-6
9. D. Pinault, T. J. O'brien, Cellular and network mechanisms of genetically-determined absence seizures, *Thalamus Relat. Syst.*, **3** (2005), 181–203. https://doi.org/10.1017/S1472928807000209

10. S. Bhattacharya, M. B. L. Cauchois, P. A. Iglesias, Z. S. Chen, The impact of a closed-loop thalamocortical model on the spatiotemporal dynamics of cortical and thalamic traveling waves, *Sci. Rep.*, **11** (2021), 14359. https://doi.org/10.1038/s41598-021-93618-6

11. P. N. Taylor, Y. Wang, M. Goodfellow, J. Dauwels, F. Moeller, U. Stephani, et al., A computational study of stimulus driven epileptic seizure abatement, *PLoS One*, **9** (2014),1–26. https://doi.org/10.1371/journal.pone.0114316

12. S. I. Amari, Characteristics of randomly connected threshold-element networks and network systems, *Proc. IEEE*, **59** (1971), 35–47. https://doi.org/10.1109/PROC.1971.8087

13. H. R. Wilson, J. D. Cowan, Excitatory and inhibitory interactions in localized populations of model neurons, *Biophys. J.*, **12** (1972), 1–24. https://doi.org/10.1016/S0006-3495(72)86068-5

14. M. Goodfellow, K. Schindler, G. Baier, Intermittent spike-wave dynamics in a heterogeneous, spatially extended neural mass model, *NeuroImage*, **55** (2011), 920–932. https://dx.doi.org/10.1016/j.neuroimage.2010.12.074

15. P. N. Taylor, J. Thomas, N. Sinha, J. Dauwels, M. Kaiser, T. Thesen, et al., Optimal control based seizure abatement using patient derived connectivity, *Front. Neurosci.*, **9** (2015), 202. https://doi.org/10.3389/fnins.2015.00202

16. S. Liu, Q. Wang, Transition dynamics of generalized multiple epileptic seizures associated with thalamic reticular nucleus excitability: A computational study, *Commun. Nonlinear Sci. Numer. Simul.*, **52** (2017), 203–213. https://doi.org/10.1016/j.cnsns.2017.04.035

17. Y. Cao, X. He, Y. Hao, Q. Wang, Transition dynamics of epileptic seizures in the coupled thalamocortical network model, *Int. J. Bifurcation Chaos*, **28** (2018), 1850104. https://doi.org/10.1142/S0218127418501043

18. L. Yan, H. Zhang, Z. Sun, Z. Shen, Control analysis of electrical stimulation for epilepsy waveforms in a thalamocortical network, *J. Theor. Biol.*, **504** (2020), 110391. https://doi.org/10.1016/j.jtbi.2020.110391

19. Z. Wang, L. Duan, The combined effects of the thalamic feed-forward inhibition and feed-back inhibition in controlling absence seizures, *Nonlinear Dyn.*, **108** (2022), 191–205. https://doi.org/10.1007/s11071-021-07178-5

20. A. Somarowthu, K. M. Goff, E. M. Goldberg, Two-photon calcium imaging of seizures in awake, head-fixed mice, *Cell Calcium*, **96** (2021), 102380. https://doi.org/10.1016/j.ceca.2021.102380

21. M. Steriade, Interneuronal epileptic discharges related to spike-and-wave cortical seizures in behaving monkeys, *Electroencephalogr. Clin. Neurophysiol.*, **37** (1974), 247–263. https://doi.org/10.1016/0013-4694(74)90028-5

22. S. Tabatabaee, F. Bahrami, M. Janahmadi, The critical modulatory role of spiny stellate cells in seizure onset based on dynamic analysis of a neural mass model, *Front. Neurosci.*, **15** (2021), 743720. https://doi.org/10.3389/fnins.2021.743720

23. L. Yan, H. Zhang, Z. Sun, Z. Cao, Z. Shen, Y. Zhao, Mechanism analysis for excitatory interneurons dominating poly-spike wave and optimization of electrical stimulation, *Chaos Interdiscip. J. Nonlinear Sci.*, **32** (2022). https://doi.org/10.1063/5.0076439

24. L. Yan, H. Zhang, Z. Sun, S. Liu, Y. Liu, P. Xiao, Optimization of stimulation waveforms for regulating spike-wave discharges in a thalamocortical model, *Chaos, Solitons Fractals*, **158** (2022), 112025. https://doi.org/10.1016/j.chaos.2022.112025

25. Y. Yu, X. Wang, Q. Wang, Q. Y. Wang, A review of computational modeling and deep brain stimulation: applications to Parkinson's disease, *Appl. Math. Mech.*, **41** (2020), 1747–1768. https://doi.org/10.1007/s10483-020-2689-9

26. O. V. Popovych, P. A. Tass, Multisite delayed feedback for electrical brain stimulation, *Front. Physiol.*, **9** (2018), 46. https://doi.org/10.3389/fphys.2018.00046

27. Z. Wang, Q. Wang, Stimulation strategies for absence seizures: targeted therapy of the focus in coupled thalamocortical model, *Nonlinear Dyn.*, **96** (2019), 1649–1633. https://doi.org/10.1007/s11071-019-04876-z

28. Y. Yu, Y. Fan, F. Han, G. Luan, Q. Wang, Transcranial direct current stimulation inhibits epileptic activity propagation in a large-scale brain network model, *Sci. China Technol. Sci.*, **66** (2023), 3628–3638. https://doi.org/10.1007/s11431-022-2341-x

29. S. Hou, D. Fan, Q. Wang, Regulating absence seizures by tri-phase delay stimulation applied to globus pallidus internal, *Appl. Math. Mech.*, **43** (2022), 1399–1414. https://doi.org/10.1007/s10483-022-2896-7

30. P. A. Tass, L. Qin, C. Hauptmann, S. Dovero, E. Bezard, T. Boraud, et al., Coordinated reset has sustained aftereffects in Parkinsonian monkeys, *Ann. Neurol.*, **72** (2012), 816–820. https://doi.org/10.1002/ana.23663

31. D. Fan, Q. Wang, Closed-loop control of absence seizures inspired by feedback modulation of basal ganglia to the corticothalamic circuit, *IEEE Trans. Neural Syst. Rehabil. Eng.*, **28** (2020), 581–590. https://doi.org/10.1109/TNSRE.2020.2969426

32. N. Sinha, J. Dauwels, M. Kaiser, S. Cash, W. M. Brandon, Y. Wang, et al., Predicting neurosurgical outcomes in focal epilepsy patients using computational modelling, *Brain*, **140** (2017), 319–332. https://doi.org/10.1093/brain/aww299

33. D. Fan, Q. Wang, J. Su, H. Xi, Stimulus-induced transitions between spike-wave discharges and spindles with the modulation of thalamic reticular nucleus, *J. Comput. Neurosci.*, **43** (2017), 203–225. https://doi.org/10.1007/s10827-017-0658-4

34. L. Yin, F. Han, Y. Yu, Q. Wang, A computational network dynamical modeling for abnormal oscillation and deep brain stimulation control of obsessive–compulsive disorder, *Cognit. Neurodyn.*, **17** (2023), 1167–1184. https://doi.org/10.1007/s11571-022-09858-3

35. X. Wang, Y. Yu, F. H, Q. Wang, Beta-band bursting activity in computational model of heterogeneous external globus pallidus circuits, *Commun. Nonlinear Sci. Numer. Simul.*, **110** (2022), 106388. https://doi.org/10.1016/j.cnsns.2022.106388

36. Y. Yu, Y. Fan, S. Hou, Q. Wang, Optogenetic stimulation of primary motor cortex regulates beta oscillations in the basal ganglia: A Computational study, *Commun. Nonlinear Sci. Numer. Simul.*, **117** (2023), 106918. https://doi.org/10.1016/j.cnsns.2022.106918

37. K. B. Baker, E. B. Plow, S. Nagel, A. B. Rosenfeldt, R. Gopalakrishnan, C. Clark, et al., Cerebellar deep brain stimulation for chronic post-stroke motor rehabilitation: a phase I trial, *Nat. Med.*, **29** (2023), 2366–2374. https://doi.org/10.1038/s41591-023-02507-0

38. T. Loddenkemper, A. Pan, S. Neme, K. B. Baker, A. R. Rezai, D. S. Dinner, et al., Deep brain stimulation in epilepsy, *J. Clin. Neurophysiol.*, **18** (2001), 514–532. https://doi.org/10.1097/00004691-200111000-00002

39. D. Fan, Z. Wang, Q. Wang, Optimal control of directional deep brain stimulation in the parkinsonian neuronal network, *Commun. Nonlinear Sci. Numer. Simul.*, **36** (2016), 219–237. https://doi.org/10.1016/j.cnsns.2015.12.005

40. J. J. Lippman-Bell, C. Zhou, H. Sun, J. S. Feske, F. E. Jensen, Early-life seizures alter synaptic calcium-permeable AMPA receptor function and plasticity, *Mol. Cell. Neurosci.*, **76** (2016),11–20. https://doi.org/10.1016/j.mcn.2016.08.002

41. C. H. Tran, M. Vaiana, J. Nakuci, A. Somarowthu, K. M. Goff, N. Goldstein, et al., Interneuron desynchronization precedes seizures in a mouse model of Dravet syndrome, *J. Neurosci.*, **40** (2020), 2764–2755. https://doi.org/10.1523/JNEUROSCI.2370-19.2020

42. A. Satlin, L. Kramer, A. Laurenza, Development of perampanel in epilepsy, *Acta Neurol. Scand.*, **127** (2013), 3–8. https://doi.org/10.1111/ane.12098

43. M. V. Sysoeva, A. Lüttjohann, G. V. Luijtelaar, I. V. Sysoev, Dynamics of directional coupling underlying spike-wave discharges, *Neuroscience*, **314** (2016), 75–89. https://doi.org/10.1016/j.neuroscience.2015.11.044

44. Y. Yu, F. Han, Q. Wang, Q. Y. Wang, Model-based optogenetic stimulation to regulate beta oscillations in Parkinsonian neural networks, *Cognit. Neurodyn.*, **16** (2022), 667–681. https://doi.org/10.1007/s11571-021-09729-3

45. M. Lv, J. Ma, Multiple modes of electrical activities in a new neuron model under electromagnetic radiation, *Neurocomputing*, **205** (2016), 375–381. https://doi.org/10.1016/j.neucom.2016.05.004

AIMS Press